REPORT DOCUMENTATION PAGE

Form Approved OMB NO. 0704-0188

1. REPORT DATE (DD-MM-YYYY)	2. REPORT TYPE	3. DATES COVERED (From - To)
	New Reprint	-

4. TITLE AND SUBTITLE

A Novel Method for Dynamic Short-Beam Shear Testing of 3D Woven Composites

5a. CONTRACT NUMBER

W911NF-08-1-0120

5b. GRANT NUMBER

5c. PROGRAM ELEMENT NUMBER

611102

6. AUTHORS

T. R. Walter, G. Subhash, B. V. Sankar, M. C. Song, C. F. Yen

5d. PROJECT NUMBER

5e. TASK NUMBER

5f. WORK UNIT NUMBER

7. PERFORMING ORGANIZATION NAMES AND ADDRESSES

University of Florida Office of Engineering Resea
339 Weil Hall

Gainesville, FL   32611   -6550

8. PERFORMING ORGANIZATION REPORT NUMBER

9. SPONSORING/MONITORING AGENCY NAME(S) AND ADDRESS(ES)

U.S. Army Research Office
P.O. Box 12211
Research Triangle Park, NC 27709-2211

10. SPONSOR/MONITOR'S ACRONYM(S)

ARO

11. SPONSOR/MONITOR'S REPORT NUMBER(S)

52873-EG.11

12. DISTRIBUTION AVAILIBILITY STATEMENT

Approved for public release; distribution is unlimited.

13. SUPPLEMENTARY NOTES

The views, opinions and/or findings contained in this report are those of the author(s) and should not contrued as an official Department of the Army position, policy or decision, unless so designated by other documentation.

14. ABSTRACT

A new test method for performing dynamic short-beam shear tests using a momentum trapped Hopkinson pressure bar is proposed. Angle-interlock 3D woven composite specimens were tested under quasi-static and dynamic loading conditions to determine the effect of loading rate on damage evolution. The equilibrium condition in the composite specimen under dynamic loads was verified using finite element analysis of the experiment. A high speed camera was used to capture delamination initiation and propagation during both quasi-static and dynamic

15. SUBJECT TERMS

Highstrainratetesting.Hopkinsonpressurebar.3D woven composites.Interlaminar shear strength.Shortbeam shear

16. SECURITY CLASSIFICATION OF:			17. LIMITATION OF ABSTRACT	15. NUMBER OF PAGES	19a. NAME OF RESPONSIBLE PERSON
a. REPORT	b. ABSTRACT	c. THIS PAGE			Bhavani Sankar
UU	UU	UU	UU		19b. TELEPHONE NUMBER
					352-392-6749

Report Title

A Novel Method for Dynamic Short-Beam Shear Testing of 3D Woven Composites

ABSTRACT

A new test method for performing dynamic short-beam shear tests using a momentum trapped Hopkinson pressure bar is proposed. Angle-interlock 3D woven composite specimens were tested under quasi-static and dynamic loading conditions to determine the effect of loading rate on damage evolution. The equilibrium condition in the composite specimen under dynamic loads was verified using finite element analysis of the experiment. A high speed camera was used to capture delamination initiation and propagation during both quasi-static and dynamic experiments. Analysis of the load-deflection curves and the high speed images revealed a good correlation between the modes of damage initiation and propagation with the features in the loading response. The apparent inter-laminar shear strength
and the bending stiffness increased with rate of loading. While the damage was observed to propagate at a relative steady rate during quasi-static loading, the high rate of energy input during dynamic loading resulted in a rapid propagation of damage and a subsequent loss of stiffness in the composite as noted in the load-deflection curve

REPORT DOCUMENTATION PAGE (SF298)
(Continuation Sheet)

Continuation for Block 13

ARO Report Number   52873.11-EG
A Novel Method for Dynamic Short-Beam Shear   ...

A Novel Method for Dynamic Short-Beam Shear Testing of 3D Woven Composites

**T.R. Walter · G. Subhash · B.V. Sankar ·
M.C. Song · C.F. Yen**

Abstract A new test method for performing dynamic short-beam shear tests using a momentum trapped Hopkinson pressure bar is proposed. Angle-interlock 3D woven composite specimens were tested under quasi-static and dynamic loading conditions to determine the effect of loading rate on damage evolution. The equilibrium condition in the composite specimen under dynamic loads was verified using finite element analysis of the experiment. A high speed camera was used to capture delamination initiation and propagation during both quasi-static and dynamic experiments. Analysis of the load-deflection curves and the high speed images revealed a good correlation between the modes of damage initiation and propagation with the features in the loading response. The apparent inter-laminar shear strength and the bending stiffness increased with rate of loading. While the damage was observed to propagate at a relative steady rate during quasi-static loading, the high rate of energy input during dynamic loading resulted in a rapid propagation of damage and a subsequent loss of stiffness in the composite as noted in the load-deflection curve.

Keywords High strain rate testing · Hopkinson pressure bar · 3D woven composites · Interlaminar shear strength · Short beam shear

T.R. Walter · G. Subhash (✉) · B.V. Sankar · M.C. Song
Mechanical and Aerospace Engineering, University of Florida,
Gainesville, FL 32611, USA
e-mail: subhash@ufl.edu

C.F. Yen
U.S. Army Research Laboratory-RDRL-WMM-B,
Aberdeen Proving Ground,
Aberdeen, MD 21005-5069, USA

Introduction

The use of laminated composite materials in the design of structures has increased in recent years due to their high strength to weight ratio and increased performance. However, laminated composite plates often have low-strength in the thickness direction relative to the in-plane directions which leads to a high propensity for damage and interlaminar failure. In particular, impact damage produces high inter-laminar stresses which induce delamination damage [1, 2]. This damage may easily propagate further as the composite structure is exposed to normal (quasi-static) operating conditions [3, 4]. This behavior has been well documented and many approaches have been used to increase the delamination resistance of composites. These methods include the addition of through-thickness reinforcements such as z-pinning [5, 6], 3D weaving [1, 7], toughened epoxies [8–10], and nano-reinforcements [11, 12]. To determine the effectiveness of these techniques on inter-laminar strength, several test methods have been utilized. The double cantilever beam (DCB) test [13] has been used to investigate the mode I fracture toughness of composites whereas the end-notch flexure (ENF) test [14] has been used to evaluate mode II fracture toughness. Both methods require a pre-crack either produced during manufacture by inserting a Teflon® tape or by cutting a crack into the edge of a sample. When performing DCB tests on high strength composites (such as stitched or 3D woven composites), premature failure often occurs due to the compressive stress caused by bending. To ensure proper failure, a test method has been developed [15] in which a combination of axial and transverse loads are applied to the test specimen. The axial tensile force prohibits the compressive bending failure while the transverse load produces mode I fracture. Other methods have also been developed to produce mixed-mode loading [16]. The short beam shear (SBS) test was developed to

determine the inter-laminar shear strength of composites [17]. Unlike the previous methods, the SBS test does not require a pre-crack. To perform a short beam shear test, a relatively thick specimen is subjected to three-point bending [7]. The large specimen thickness relative to the test span creates a substantial inter-laminar shear stress which results in delamination initiation and propagation. The peak stress is calculated assuming a parabolic stress distribution through the thickness and is used to determine the inter-laminar shear strength (ILSS) of the composite. However, the large contact stresses between the loading point and the composite often cause excessive crushing at the contact points leading to premature failure of the composite, while the simplified stress distribution assumption often misrepresents the true ILSS. For this reason, the strength determined from SBS tests are often referred to as the apparent inter-laminar shear strength and can be used in the assessment of relative performance potential between composites rather than as a material property.

Since delamination is a primary mode of failure in composites during impact or impulse loading, it is important to characterize the response under dynamic loading conditions. Several techniques exist to perform low velocity impact tests. The most common technique is the drop tower test where a given impact energy is imparted to a composite specimen. A variety of composite structures including stitched and 3D woven composites have been tested using this method [18–20] at various impact velocities. Due to the combination of velocity and mass to impart desired impact energy, the rate of loading is often non-uniform throughout the impact event. Also, the total displacement of the specimen is not controlled and consequently often varies for each test. In some cases these qualities may be undesirable and therefore alternative methods may be required. Damage in composites can be evaluated using non-destructive techniques including ultrasonic measurements. Additionally, the effect of induced damage during impact tests are often evaluated using post mortem quasi-static compression after impact (CAI) tests [21, 22]. Another popular method to conduct dynamic impact tests on composites uses gas guns for the determination of impact damage resistance [23, 24]. Similar to drop tower tests, ballistic impact relies on projectile mass and velocity to impart a certain level of impact energy. In both of these tests it is difficult to control or predict displacement during impact. A third method used to perform dynamic tests on composites is the split Hopkinson pressure bar (SHPB) which is commonly used to evaluate high strain rate response of many different engineering materials [25, 26]. Traditional SHPB test utilizes elastic longitudinal stress waves traveling in long high strength steel bars to perform high strain rate tests. The sample shapes may be varied to perform a variety of different tests. The SHPB has been used to determine the dynamic compressive strength [27, 28], tensile strength [29], and shear strength [30, 31] of composites.

Although numerous methods exist for delamination testing of composites, few methods exist specifically for determination of delamination strength or inter-laminar shear strength under dynamic loads. Such methods are necessary to understand the dynamic response of composites under impact loads. In this manuscript a novel test method is proposed to determine the apparent delamination strength of composites subjected to high rate of loading with a time scale on the order of few hundred microseconds. Experiments under static (low strain rate) loads were also conducted for comparison of delamination strength and induced fracture. The proposed technique demonstrates an alternative to drop tower testing by producing repeatable deformations at relatively constant velocities. This test method allows for a better comparison of quasi-static and dynamic results. A finite element study was conducted to verify several assumptions used in the evaluation of the tests results.
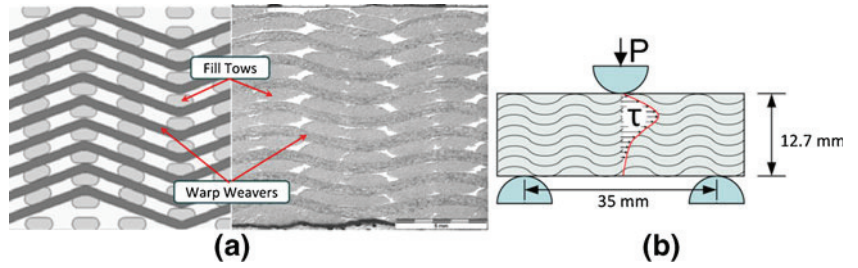
Experimental Procedure

To evaluate the effect of loading rate on the inter-laminar shear strength of a 3D woven composite, short-beam shear tests were performed at several rates of loading using both a universal testing machine and a modified Hopkinson pressure bar (mHPB) apparatus. The test specimens were cut from composite panels supplied by the US Army Research Laboratory, Aberdeen Proving Ground, MD. A high speed camera was used during both quasi-static and dynamic tests to capture the deformation and the modes of damage in the composite.

Materials

Angle-interlock 3D woven composite panels, manufactured by TEAM Inc., Woonsocket, RI, were used in this investigation. The preforms were woven from S-2 glass fiber and consolidated with SC-15 epoxy using vacuum assisted resin transfer molding. The weaving pattern consisted of 10 fill tows and 9 warp weavers. Each warp weaver is woven around two layers of fill tows and the weaving pattern is shifted by one column of fill for each row of weavers. The pattern repeats every four rows of weavers and results in 19 interwoven layers of S-2 glass/SC15 composite. Using rule of mixtures the total fiber volume was estimated to be 48 % of the total composite volume. The architectural details as well as an optical micrograph are provided in Fig. 1(a). The original composite panels measured 660 mm x 700 mm and were nominally 12.7 mm thick. The as-received panels were

Fig. 1 (**a**) Schematic and optical micrograph of 3D woven angle interlock composite specimen, and (**b**) Schematic of static short beam shear test fixture. The shear stress distribution along the center line is also shown

sectioned into smaller 150 mm x 150 mm tiles. These tiles were then cut using a high speed diamond sectioning saw into the desired test coupons with approximate dimensions of 50 mm×20 mm. The 20 mm dimension was chosen to include at least two unit cells in the width of the specimen. The exact dimensions of each specimen varied slightly due to variability in the manufacturing process. To remove damage induced during sectioning, the edges of the specimens were polished using standard metallographic techniques.

Static Short Beam Shear Test

The short beam shear [17] (SBS) test method was used to evaluate the apparent inter-laminar shear strength (ILSS) of the 3D woven composite at different rates of loading. This test method, shown in Fig. 1(b), uses a three-point loading fixture to perform bending tests on a test specimen with a relatively small length to thickness ratio. This geometry creates a large inter-laminar shear stress within the specimen on either side of the central load point and promotes delamination damage. The inter-laminar shear strength can be approximated using the following formula [17]:
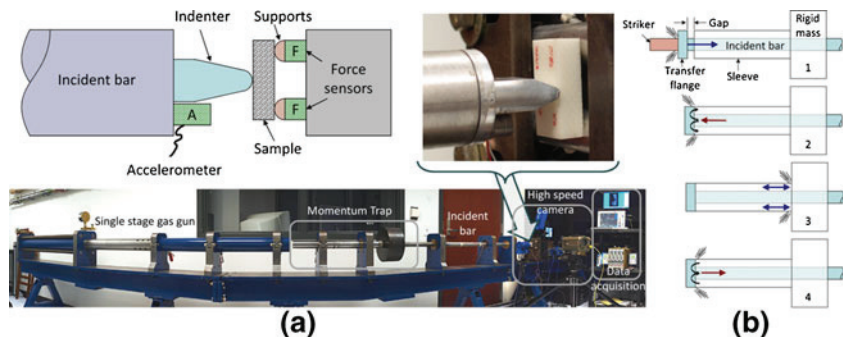
$$ILSS = 0.75P_B/bd \qquad (1)$$

where P_B is the peak bending load, b is the width, and d is the thickness of the specimen. Quasi-static SBS tests were first performed on several specimens at various rates of loading using a MTS® servo hydraulic universal testing machine. Figure 1(b) shows a schematic of the SBS test fixture with a fixed support span of 35 mm. Specimens were tested at three different rates of loading; 0.0001 m/s, 0.001 m/s, and 0.01 m/s. A 111 kN load cell was used to

measure the force applied to each specimen while the deflection was measured using the LVDT of the MTS® test machine. A preload of 200 N was used to remove any slack between the fixtures and the specimen.

Dynamic Short Beam Shear Test

A modified Hopkinson pressure bar apparatus was used to perform dynamic short beam shear (dSBS) tests. This apparatus consists of three major components; a single stage gas gun, a 38.1 mm diameter incident bar with a momentum trap [25, 26, 32] at one end and an aluminum indenter at the other end, and a rigid anvil which serves to support the specimen and the force sensors. The bar material is a precipitation hardened steel which has high yield strength, even in an annealed state. A schematic of the test system is shown in Fig. 2(a). The composite test specimens were supported on two 19 mm half-cylindrical support rods spanning approximately 38 mm and clamped to the rigid anvil. Two PCB® 210b dynamic force sensors are placed between the anvil and the supports (one for each support). These force sensors can measure a combined maximum load of 44.5 kN with a frequency response of 75 kHz. The sensors are conditioned using two Kistler 5010 charge amplifiers and are clamped in place with a preload of 2.2 kN. A 45° wedge shaped indenter with a tip radius of 2.4 mm is threaded into the end of the incident bar. The indenter was made from 7068 Aluminum to reduce the indenter mass, while maintaining sufficient stiffness and strength to resist forces during loading. A 350 Ω foil resistive strain gage was bonded near the midspan of the incident bar and was used to monitor shape, amplitude and duration of the incident wave.

Fig. 2 (**a**) Dynamic short beam shear test fixture using a modified Hopkinson bar apparatus. Detail of supports, load cell placement and accelerometer are shown in the schematic and an enlarged photo above. (**b**) A schematic is shown detailing the process of the momentum trap technique

The strain gage signal was conditioned and amplified using a Vishay 2310b dynamic strain conditioner. A pulse shaping technique [25, 26, 33] was implemented by placing a 0.8 mm thick, 19 mm diameter copper disk between the striker bar and the incident bar before each test. This technique results in a long rise time in the incident pulse which decreases acceleration of the bar and reduces signal noise from the strain gage and the force sensors. Although the acceleration during impact is reduced due to pulse shaping, the magnitude may still be in excess of 200,000 m/s². To measure this high acceleration, a PCB® 350B21 ICP shock accelerometer was attached to the end of the incident bar next to the indenter tip (see the schematic in Fig. 2(a)). The accelerometer has a maximum capacity of 980,000 m/s² and a resonance frequency of over 200 kHz. This sensor was conditioned using a PCB® 482A16 signal conditioner. Data was collected from the strain gage, force sensors, and accelerometer using a LDS-Nicolet Sigma 90–8 oscilloscope with a sample rate of 5 MS/s.

To conduct the dSBS test, a 600 mm striker bar was launched from the gas gun toward the incident bar. Upon impact, an elastic uniaxial compressive stress wave was generated in the incident bar with an amplitude and duration proportional to the velocity of impact and the length of the striker bar, respectively. This compression wave then travels down the length of the incident bar until it reaches the indenter/specimen interface. The compressive wave causes the flexure of the composite and, due to the low impedance of the specimen, reflects back as a tensile wave. In a traditional Hopkinson bar, once the loading is complete the reflected tensile stress pulse travels back toward the striker-incident bar interface and reflects back again into the incident bar as a compressive wave, which travels toward the indenter and causes a second impact on the specimen. This is often an undesirable consequence of the traditional Hopkinson bar testing.

If specimens were to be recovered after the test and analyzed either through microscopy or further experimental testing, it is important that the damage induced during testing is limited to a single impact. To prevent repeated loading, a momentum trapping technique has been developed known as recovery Hopkinson pressure bar technique [26, 32]. This technique has been used to induce controlled damage in brittle materials [34] and to determine dynamic hardness of several ceramics [25, 35, 36]. A variation of this technique was used in this research. The recovery Hopkinson bar uses a 'momentum-trap' which consists of three components, a transfer flange, a sleeve, and a rigid mass. The transfer flange is either formed or machined onto the end of the incident bar. The flange and sleeve are impedance matched to the incident bar while the rigid mass is required to be large enough to act as a rigid surface. The technique used in this research uses a controlled gap placed between the flange and the sleeve. The details of this technique and the operational principle are described below and are shown as a schematic in Fig. 2(b).

1) Upon the striker bar impact a compression wave is generated in the incident bar and at the end of the pulse duration, the gap between the flange and the sleeve is closed which then engages the momentum trap.
2) The pulse reaches the indenter and after loading the specimen reflects back as a tensile wave and returns to the striker end of the incident bar. The stress wave is then transferred by means of the flange into the sleeve as a compressive wave.
3) Upon reaching the rigid mass the stress wave reflects back into the sleeve as a compressive wave due to the large impedance mismatch between the sleeve and the rigid mass. This compressive wave then returns to the transfer flange.
4) Upon reaching the flange the compressive wave transfers into the incident bar as a tensile wave which then travels toward the indenter (or the specimen) and subsequently retracts the indenter from the composite specimen.

The wave then repeatedly reflects back and forth in the incident bar such that it is always tensile while traveling towards the specimen so that the incident bar is incrementally retracted causing the indenter to move away from the sample. The result is a single dynamic loading on the composite specimen followed by the retraction of the incident bar.

In this paper three possible methods to determine the displacement of the wedge indenter were examined: (i) a shock accelerometer mounted on the incident bar next to the indenter, (ii) a strain gage bonded on the incident bar and (iii) high speed imaging of the indenter motion during the test. The shock accelerometer measures the axial acceleration, from which velocity and displacement of the indenter were determined by successive integration of the acceleration signal. Integration naturally smoothes the noisy acceleration signal to produce smooth velocity and displacement profiles. The second method relies on the measurement of the stress wave using the strain gage on the incident bar. The strain measured at a point on the bar is related to the particle velocity at that cross section through the following relation:

$$U_p = C\varepsilon \tag{2}$$

Were ε is the recorded strain profile of the incident pulse and C is the longitudinal wave speed in the bar (~5000 m/s) which may be determined by analyzing the time between two successive wave reflections and the distance the wave travels in the incident bar. The use of steel for the bar material reduces the effects of the dispersion on the incident/reflected pulses. In addition the use of pulse shaping reduces the high frequency components of the stress wave

related to Pochhammer-Chree oscillations which further reduces dispersion and therefore these effects may be neglected. Using this assumption and the above relation, it can be shown that the velocity at the end of the incident bar (i.e., velocity of the indenter) may be determined using the incident (ε_I) and reflected (ε_R) strain signals measured at the midspan of the incident bar using the following equation [37]:

$$V = C(\varepsilon_I - \varepsilon_R) \qquad (3)$$

Once the velocity is determined the signal may be integrated to determine the displacement at the end of the incident bar. For dSBS tests, the impedance of the specimen is negligibly small compared to the impedance of the steel incident bar. This results in very little loss in energy during the loading of the specimen and therefore the reflected stress wave is almost equal in amplitude to the incident wave but opposite in sign (i.e., $\varepsilon_R = -\varepsilon_I$). Using this assumption we may simplify (equation (3)) to estimate the velocity at the end of the bar as

$$V = 2C\varepsilon_I \qquad (4)$$

This equation is useful to quickly determine the velocity of the impact loading and may also be integrated to find the displacements at the end of the incident bar for comparison with other methods.

Finally, we have used a high speed digital camera (Phantom v710, Vision Research, Wayne, NJ) to image the specimen deformation during the impact. The camera control software has the capacity to manually track pixels of images taken during the test. Using the measured thickness of the specimen the images are calibrated to the proper scale. The displacement of the indenter tip during the dynamic bend test can then be determined using the images at different time intervals. The minimum measurable displacement is limited by the resolution of the images and the scaling of the region of interest. In this case the resolved displacement is limited to 0.108 mm increments. However, the limited number of data points, and the small relative displacements results in significant quantization error, making it difficult to accurately determine the velocity profile from the high speed images.

Recall that the load applied by the wedge indenter is measured by two force sensors beneath the two supports. The force measured by each sensor is half the applied load during dSBS tests. The signals from the two force sensors are summed to obtain the load-time curve. The displacement-time profiles (either from strain gages, accelerometer or high speed images) are then matched to the load-time profile to obtain the load–displacement curve for each dSBS test. From these curves the ILSS of the composite specimens subjected to a single dynamic loading is determined using (equation (1)).
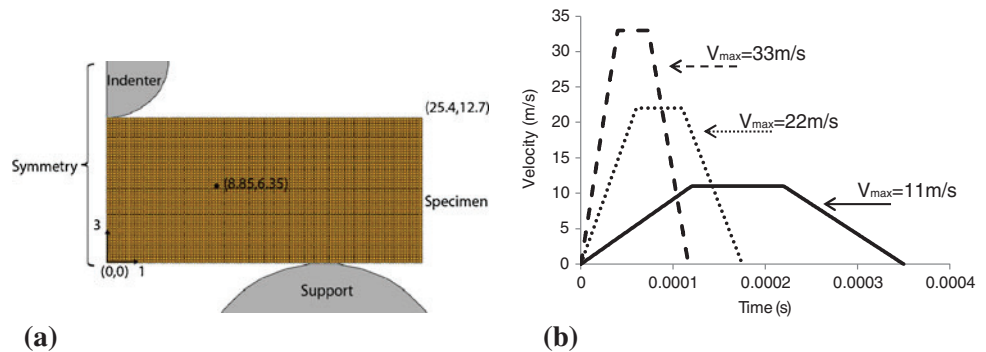
High Speed Photography

During the quasi-static and dynamic SBS tests, high speed imaging was used to record damage modes and damage evolution in the specimen. The camera was configured with a frame size of 1024×400 pixels and a frame rate of 18,000 fps during the static testing. The frame size was reduced for the dSBS tests to 256×376 pixels which allowed the frame rate to increase to 54,000 fps. During both cases a Carl Zeiss Makro planer 100 mm lens was used with the aperture set to f/8.

Finite Element Modeling

Equation (1) used in this study in conjunction with the measured impact force for estimating ILSS implicitly assumes that the specimen is in quasi-static equilibrium and any dynamic (inertia) effects are neglected. In order to verify this assumption Finite Element Analysis (FEA) of the impact test was performed. The analysis was simplified by utilizing the symmetry of the test and therefore only one half of the dSBS specimen was modeled as shown in Fig. 3(a). In addition, the specimen was homogenized as an orthotropic elastic material with properties given in Table 1 [38]. The use of fully elastic model removes any material rate dependency and focuses the study on the effect of inertia and wave mechanics. The FEA study included three rates of dynamic impact as well as quasi-static loading to determine how loading rate affects the outcome of the analysis.

Fig. 3 (a) 2D FE model for SBS test and (b) Velocity profiles of indenter for dynamic loading

Table 1 Material properties of the DSBS specimen for FEA [38]

Density (kg/m³)	2300
$E_1 = E_2$ (GPa)	27.5
E_3 (GPa)	11.8
$G_{13} = G_{23}$ (GPa)	2.14
G_{12} (GPa)	2.9
$v_{13} = v_{23}$	0.4
v_{12}	0.11

The commercial FE software codes, Abaqus Standard® and Abaqus Explicit® were used for the quasi-static and dynamic loading, respectively. The specimen was modeled using approximately 32,000 four-node plane strain elements with reduced integration (CPE4R), and the specimen thickness was set at 20 mm. The indenter and the support were modeled as rigid bodies.
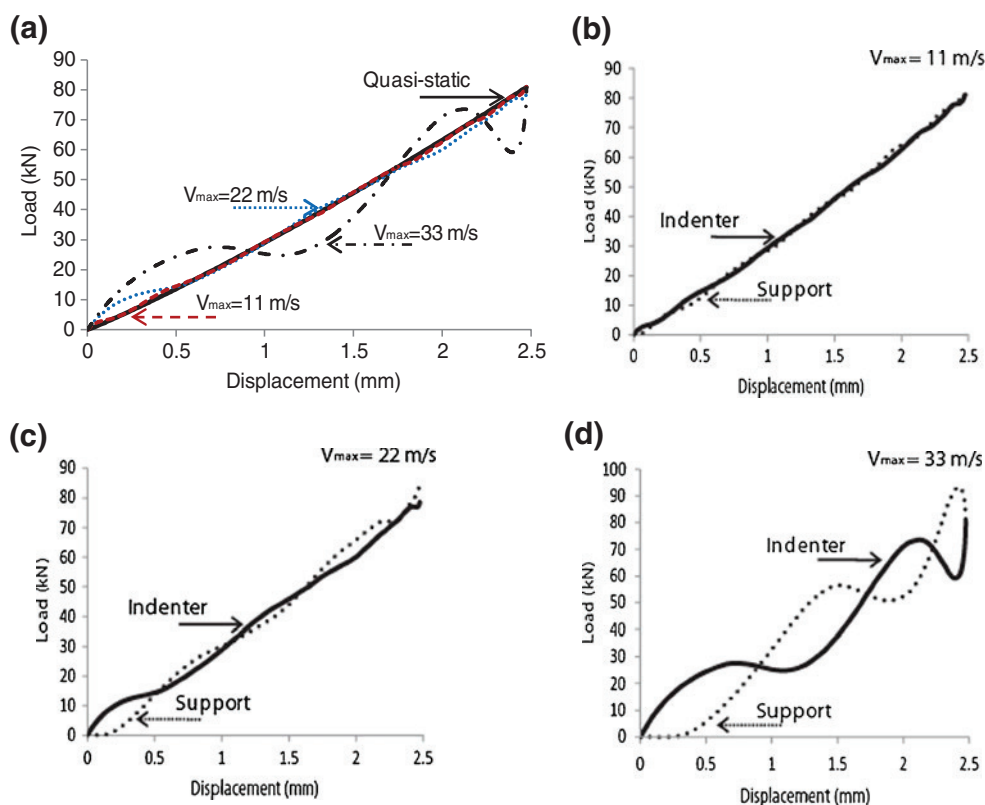
Dynamic loading was simulated using three different impact velocities, 11, 22 and 33 m/s. The maximum impact velocity of the experiments corresponds to the lowest rate, 11 m/s. The velocity profiles for the three impact simulations are depicted in Fig. 3(b). The shape of the profiles was chosen such that they closely resemble the experimentally measured profile discussed below. The duration of each profile was modeled to result in a final displacement of 2.5 mm. This displacement, which can be determined as the area under the v-t diagram, is consistent with the experimental results. Both the impact force (reaction force on the indenter) and the support reaction were monitored for each time increment. In the FEA the displacement of the rigid indenter was controlled by the velocity profile up to 2.5 mm under the displacement control. The time step for explicit analysis was calculated automatically by the FE program and it was in the order of 10^{-8} s.
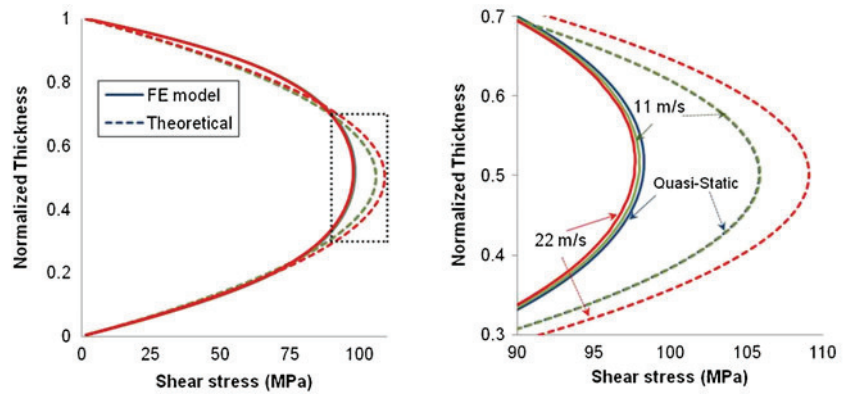
The reaction force curves determined at the indenter (impact force) are shown in Fig. 4(a). The deviation of the dynamic loading curves from the quasi-static results indicates the effects of inertia on the load histories. From these curves it was observed that up to 22 m/s the effect of inertia may be neglected. At 33 m/s this effect becomes much more significant reducing the accuracy of the results.

Next the reaction force at the support is compared with the impact force at the indenter to verify the quasi-static equilibrium. The results for the each of the dynamic loading simulations are shown in Fig. 4(b-d) (note that the results for quasi static loading were not analyzed as it is in static-equilibrium). If the specimen is in equilibrium the reaction forces at the indenter and the total force at the supports should be equal for the geometry analyzed. From Fig. 4(b) it can be noted that equilibrium is satisfied during impact with at a velocity of 11 m/s. At 22 m/s impact velocity (Fig. 4(c)), the two forces varied at the beginning of impact event however after approximately 0.5 mm of deflection, equilibrium is reached. It is observed from Fig. 4(d) that equilibrium is never fully satisfied when loaded at a rate of 33 m/s.

Fig. 4 (**a**) Load-displacement curves at the indenter and (**b-d**) comparison of load curves for indenter and support at various rates of loading

Fig. 5 (a) Transverse shear stress distribution in the specimen at a plane midway between the indenter and the support and (b) Enlarged view of the shear stress distribution near the center of the cross section (Note: the theoretical results for quasistatic and 11 m/s are almost identical)
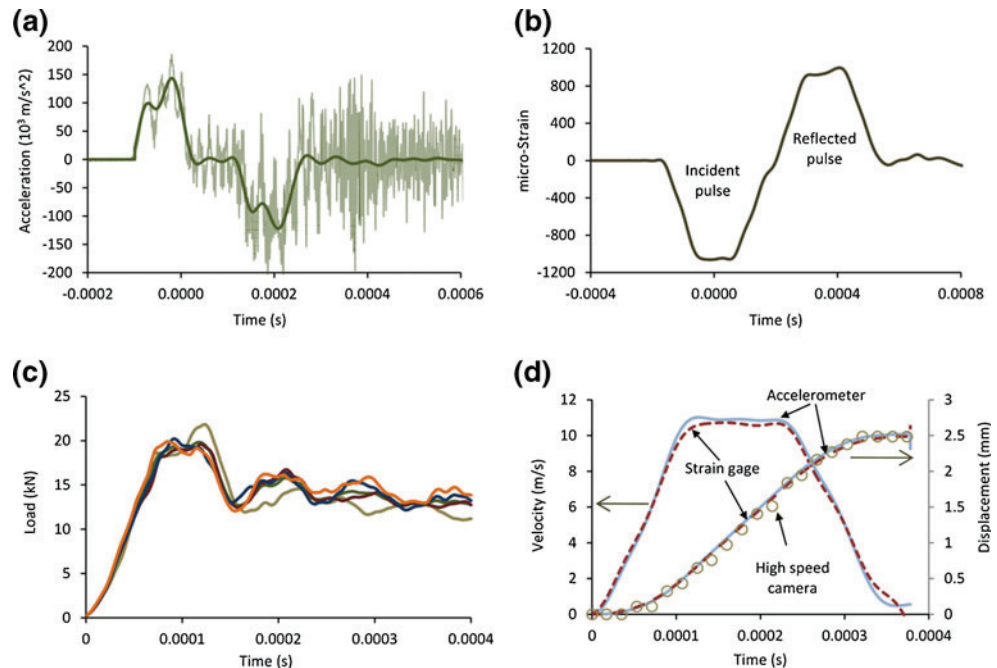

Next the through thickness transverse shear stress profile was examined for the quasi-static, 11 m/s and 22 m/s results. Since the results from 33 m/s impact were previously shown to be invalid, due to a state of non-equilibrium, it was neglected from this analysis. These profiles were determined at a point on a plane midway between the support and indenter (as shown in Fig. 3). The purpose of this comparison is to evaluate the effect of loading rate on the response of the specimen and compare the FEA profiles with the theoretical profile given by the equation $\tau = VQ/It$, where V is shear force, Q is first moment of area , I is moment of inertia and t is thickness, which is the basis for (equation (1)). The profiles were compared for a central deflection of 1.5 mm and are shown in Fig. 5. The FEA profiles are shown as solid lines while theoretical profiles are shown as dashed lines. It is apparent from Fig. 5(a) that there is only a slight deviation between quasi-static and dynamic shear stress profiles. This deviation is shown in an enlarged view in Fig 5(b). The theoretical results over predict the
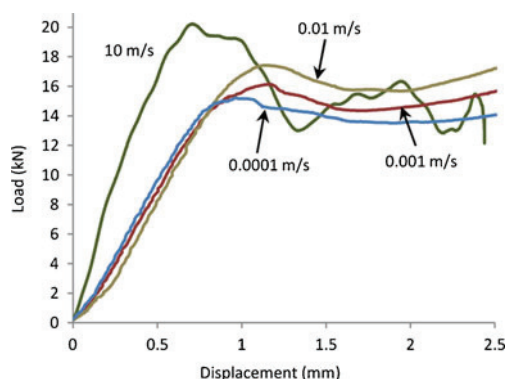
FEA shear stress by approximately 8 % for quasistatic loading as well as for a loading rate of 11 m/s, and by 11 % for a loading rate of 22 m/s. As mentioned previously the actual shear stress is often much different than what is predicted using (equation (1)) and therefore is often used to compare different architectures. These plots reveal that it is possible to compare results from static tests with the dynamic tests at rates up to 11 m/s. Even at 22 m/s the deviation between the quasistatic and dynamic results is only around 3 %. Thus, the specimen equilibrium can be maintained under dynamic loads until an impact velocity of 11 m/s and hence the present method (equation (1)) of estimating the ILSS of the material could be considered valid.

Results

Typical signals from the shock accelerometer, strain gage, and force sensors during a dSBS test are shown in Fig. 6(a-c). The

Fig. 6 (a) Typical acceleration signal (*bold line* is filtered signal), (b) strain profile at midpoint of the incident bar, (c) load-time profile, and (d) comparison of velocity and displacement profiles calculated from accelerometer (*solid line*), and strain gage signal (*dashed line*), and displacements from high speed images (*circles*)

Fig. 7 Representative load–displacement response of angle interlock 3D woven composite for quasi-static and dynamic rates of loading

load–displacement response of the composite specimen during the dynamic impact test was obtained from these signals. It was observed that the acceleration data (shown in Fig. 6(a)) contains a large amount of noise. The noise may be reduced using a digital filter to obtain a smooth acceleration curve as shown by a bold line in Fig. 6(a). However, the successive integration of the original acceleration signal reduces the noise resulting in smooth velocity and displacement profiles as shown in Fig. 6(d) without the need for digital filters. Using the strain gage signal (Fig. 6(b)) and (equation (4)), the velocity profile of the indenter tip was calculated and compared to the velocity profile from the accelerometer signal in Fig. 6(d). This profile was then integrated to determine the displacement-time response. Lastly, the high speed images captured during the test were properly scaled and used to determine the displacement of the indenter during loading of the specimen. Comparisons of the velocity and displacement profiles determined from the
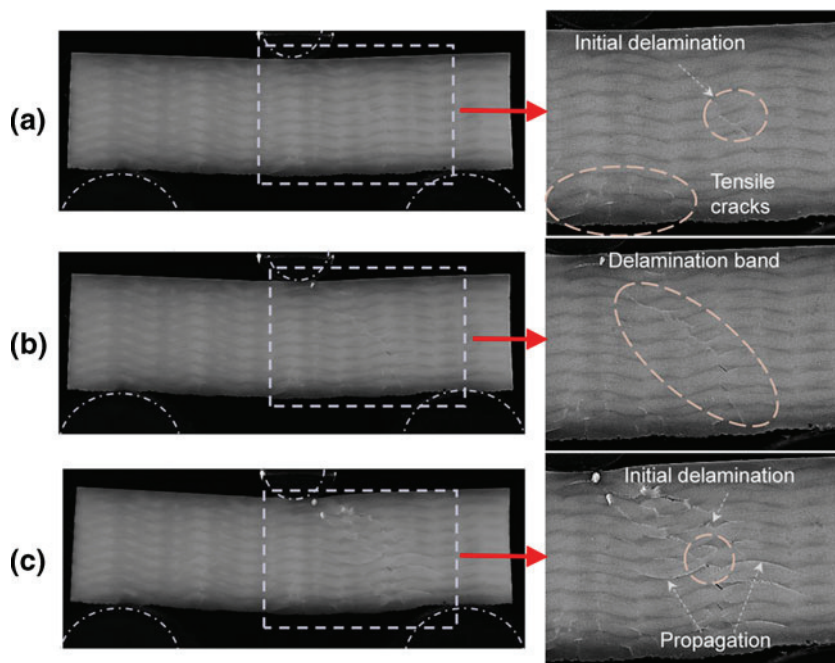
accelerometer and strain gage as well as displacements determined from the high speed images are shown in Fig. 6(d). The three methods indeed show a good agreement in displacement measurements.

The load-time profiles for five tests shown in Fig. 6(c) demonstrate the repeatability of the dSBS tests. Using these profiles and the displacement-time profiles derived from the strain signals the load–displacement curves were determined for each dSBS test. Five tests were conducted at each loading rate and the curve which best represents the average response of the composite was selected as the representative load–displacement curve. Figure 7 shows the representative curves at four different loading velocities. The features in these curves may be related to the damage modes observed in images captured using the high speed camera. These images are shown in Figs. 8 and 9 which represent typical damage patterns observed in each test. Although slight differences exist between each test, several features were repeatable and are discussed below

For both quasi-static and dynamic tests the load–displacement response in Fig. 7 shows a fairly linear region, followed by a gradual decrease in slope of the loading curve until it reaches a maximum value. It was observed that the slope of the linear region is fairly constant during quasi-static loading at the selected loading rates, but increases significantly under dynamic loading. High speed images taken during this linear response for both loading rates show small tensile cracks initiated along the bottom of the specimen as seen in Figs. 8(a) and 9(a). These cracks are due to the tensile stress induced by the bending but appeared not to affect the overall response of the load-deflection curve.
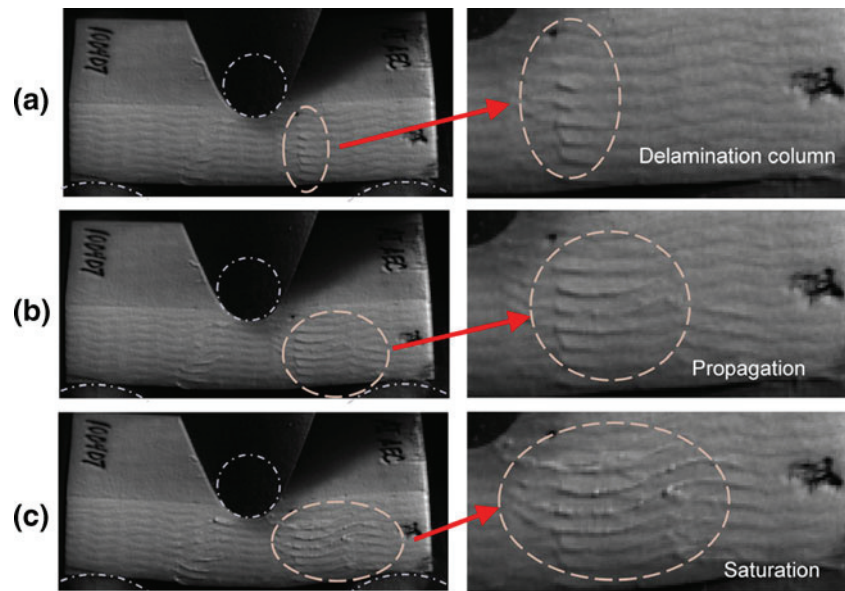
After the linear region the load plateaus for a short displacement which is more pronounced in the dynamic

Fig. 8 High speed images of quasi-static SBS test at 0.01 m/s. Magnified images show detail of crack formation including: (**a**) tensile cracks near the bottom surface, (**b**) a band of delamination cracks in the center, and (**c**) delamination propagation

Fig. 9 High speed images of dSBS test at 10 m/s. Magnified images show details of (**a**) damage formation, (**b**) propagation, and (**c**) saturation of damage between indenter and support

response. The incidence of this plateau response coincides with the initiation of delamination micro-cracks within the composite. The high speed images of the 0.01 m/s test, shown in Fig. 8(a), reveal additional tensile cracks and delamination cracks initiating midway between the indenter and the support. As the material is further deformed additional delamination cracks initiate between the warp weavers and fill tows along an inclined band extending from the indenter to the support as shown in Fig. 8(b). The dSBS images, on the other hand, show a column of delamination cracks which form near the center of the specimen as shown in Fig. 9(a). While these cracks were concentrated on one side, delamination cracks were also observed on both sides of the indenter.

As the displacement increases, the stiffness continues to drop with further increase in delamination crack length. After a displacement of around 1.25 mm the quasi-static load decreases gradually indicating a further loss in stiffness. During this loading period the delamination cracks which were formed previously, now propagate over a large distance (shown in Fig. 8(c)) causing the loss in load bearing capacity as the stiffness of the specimen is significantly reduced. During dynamic tests this drop in load is much more significant, see Fig. 7. Following the crack initiation, the propagation of delamination cracks occurs rapidly as shown in Fig. 9b and results in the sudden drop in load. The rapid damage propagation and drop in load suggested a large decrease in the stiffness of the specimen.

The above behavior continues to about 2 mm of central deflection at which point the load begins to increase gradually until the test was terminated (see Fig. 7). In the dynamic tests, additional intermittent drops in load were observed during this regime; after each drop, the load increases with displacement. The increase in load could indicate that the rate of stiffness loss due to delamination has diminished, possibly due to some limitation in damage propagation. As the delamination cracks approach the supports or are hindered by the weaving structure of the composite the delamination growth will be reduced. Figures 8(c) and 9(c) show delamination damage saturation in the area between the indenter and the support region.

From these results it was observed that both stiffness and peak load increased as the rate of loading was increased from the quasi-static to the dynamic loading regime (Fig. 7). The severity of the load drop following the peak load was greater during dynamic testing compared to static loading. With the high speed images we can deduce the reason for this large drop. In static tests the damage propagated at a relatively slow rate resulting in a gradual decline in the slope of the load curve beyond the peak load. In the dynamic tests the rate of delamination damage propagation was much faster due to the higher amount of energy imparted to the specimen during the loading process. This energy is rapidly released during dynamic loading through severe delamination leading to a loss in stiffness of the specimen and sudden load drop as seen in Fig. 7.

The maximum load during each test was used to determine the ILSS (equation (1)) and an average value was determined from five tests for each loading rate. The initial

Table 2 Apparent ILSS and initial stiffness determined from short beam shear tests

Loading rate (m/s)	Apparent ILSS (MPa)	Stiffness (kN/mm)
0.0001	45.40±0.75	14.95±0.92
0.001	48.11±0.55	14.40±0.40
0.01	50.62 ±1.23	15.00±0.54
10	59.78±1.39	34.50±1.17

stiffness from the linear response was also determined from the load–displacement curves. Results from quasi-static and dynamic tests are summarized in Table 2. It can be seen that the ILSS increases as the loading rate was increased while the stiffness of the specimen only increased under dynamic loading.

The above results clearly point to the fact that delamination damage is more severe under dynamic loads than under static loads. Effective strategies are necessary to limit delamination damage in composites if they are to be successfully implemented in applications subjected to impact loads. It is also clear that to understand the effectiveness of new composite designs intended to reduce delamination damage, controlled tests such as the dSBS tests must be conducted at high rates of loading.

Summary

Results from dynamic short beam shear tests confirmed that displacement of the indenter bar may be determined accurately from stress wave magnitude measured using the strain gage attached to the incident bar. All three methods utilized here (i.e., accelerometer, strain gage, and high speed imaging) for determining displacement during the dSBS test provided consistent results. The high speed images provide a good method to validate displacement results from either the strain gage or the accelerometer. However, the limited number of data points from the high speed camera and the relatively small displacements of the indenter do not allow for an accurate determination of the velocity profile of the indenter. Strain gages provide the most affordable and the easiest method to implement while shock accelerometers of sufficient range are often limited in availability and prone to frequent damage during tests.

The interlaminar shear strength determined from quasi-static and dynamic short beam shear tests showed a steady increase as the rate of loading increased. The use of momentum trapping produced a single controlled indentation into the composite specimen. This technique allowed for the recovery of specimens subjected to a consistent and measureable level of deformation. Although this technique has been shown to produce repeatable results it is not intended to replace drop tower tests, as the latter technique is vital in the analysis of damage resistance. Instead, dynamic indentation should be seen as an additional method to further analyze the rate dependent response of composites. This method for performing dynamic short beam shear uses small specimens to quickly compare several different designs of composites. The results from quasi-static and dynamic SBS tests of 3D woven composites indicate a change in both the load–displacement response and also in the initiation and propagation of damage characteristics.

References

1. Walter TR, Subhash G, Sankar BV, Yen CF (2009) Damage modes in 3D glass fiber epoxy woven composites under high rate of impact loading. Composites Part B: Engineering 40(6):584–589
2. Sankar BV, Sun CT (1986) Low-velocity impact damage in graphite-epoxy laminates subjected to tensile initial stresses. AIAA Journal 24(3):470–471
3. Yuanjian T, Isaac DH (2008) Combined impact and fatigue of glass fiber reinforced composites. Composites Part B: Engineering 39 (3):505–512
4. Tai NH, Yip MC, Lin JL (1998) Effects of low-energy impact on the fatigue behavior of carbon/epoxy composites. Composites Science and Technology 58(1):1–8
5. Wallace BT, Sankar BV, Ifju PG (2000) Effect of z-pinning on buckling of delaminated sandwich beams. In, Atlanta, GA, USA, 2000. Collection of Technical Papers - AIAA/ASME/ASCE/AHS/ASC Structures, Structural Dynamics and Materials Conference. American Inst. Aeronautics and Astronautics Inc., Reston, VA, USA, pp 539–544
6. Mouritz AP (2007) Review of z-pinned composite laminates. Composites Part A: Applied Science and Manufacturing 38(12):2383–2397
7. Walter TR, Subhash G, Sankar BV, Yen CF (2010) Monotonic and cyclic short beam shear response of 3D woven composites. Composites Science and Technology 70(15):2190–2197
8. Varada Rajulu A, Babu Rao G, Ganga Devi L, Balaji PJ, He J, Zhang J (2003) Interlaminar shear strength of polycarbonate-toughened epoxy composites reinforced with glass rovings. Advances in Polymer Technology 22(4):373–377
9. Reeder JR (1995) Stitching vs. a toughened matrix: Compression strength effects. Journal of Composite Materials 29(18):2464–2487
10. Deng S, Ye L (1999) Influence of fiber-matrix adhesion on mechanical properties of graphite/epoxy composites: II. Interlaminar fracture and inplane shear behavior. Journal of Reinforced Plastics and Composites 18(11):1041–1057
11. Subramaniyan AK, Sun CT (2008) Interlaminar fracture behavior of nanoclay reinforced glass fiber composites. Journal of Composite Materials 42(20):2111–2122
12. Davis DC, Whelan BD (2012) An experimental study of interlaminar shear fracture toughness of a nanotube reinforced composite. Composites Part B: Engineering 42:105
13. Standard Test Method for Mode I Interlaminar Fracture Toughness of Unidirectional Fiber-Reinforced Polymer Matrix Composites (ASTM Standard D5528-01). ASTM International, West Conshohocken, PA,
14. Sankar BV, Sharma SK (1997) Mode II delamination toughness of stitched graphite/epoxy textile composites. Composites Science and Technology 57(7):729–737
15. Chen L, Ifju PG, Sankar BV (2001) A novel double cantilever beam test for stitched composite laminates. Journal of Composite Materials 35(13):1137–1149
16. Investigation of Fracture Toughness of Laminated Stitched Composites Subjected to Mixed Mode Loading (2009) http://jrp.sagepub.com/cgi/content/abstract/0731684408099407v2. Accessed January 28, 2009
17. Standard Test Method for Short-Beam Strength of Polymer Matrix Composite Materials and Their Laminates (ASTM Standard D2344/D2344M, 2000). ASTM International, West Conshohocken, PA, www.astm.org

18. Ferri R, Sankar BV (1997) Comparative study on the impact resistance of composite laminates and sandwich panels. Journal of Thermoplastic Composite Materials 10(4):304–315

19. Baucom JN, Zikry MA, Rajendran AM (2006) Low-velocity impact damage accumulation in woven S2-glass composite systems. Composites Science and Technology 66(10):1229–1238

20. Baucom JN, Zikry MA (2005) Low-velocity impact damage progression in woven E-glass composite systems. Composites Part A: Applied Science and Manufacturing 36(5):658–664

21. Sharma SK, Sankar BV (1997) Effect of stitching on impact and interlaminar properties of graphite/epoxy laminates. Journal of Thermoplastic Composite Materials 10(3):241–253

22. Yan H, Oskay C, Krishnan A, Xu LR (2010) Compression-after-impact response of woven fiber-reinforced composites. Composites Science and Technology 70(14): 2128–2136

23. Kazemahvazi S, Zenkert D, Burman M (2009) Notch and strain rate sensitivity of non-crimp fabric composites. Composites Science and Technology 69(6):793–800

24. Sevkat E, Liaw B, Delale F, Raju BB (2009) A combined experimental and numerical approach to study ballistic impact response of S2-glass fiber/toughened epoxy composite beams. Composites Science and Technology 69(7–8):965–982

25. Subhash G (2000) Dynamic Indentation Testing. In: Kuhn H, Medlin D (eds) ASM Handbook on Mechanical Testing and Evaluation, vol 8. ASM International, Materials Park

26. Nemat-Nasser S (2000) Recovery Hopkinson Bar Techniques. In: Kuhn H, Medlin D (eds) ASM Handbook on Mechanical Testing and Evaluation, vol 8. ASM International, Materials Park

27. Dee AT, Vinson JR, Sankar B (2001) Through-thickness stitching effects on graphite/epoxy high-strain-rate compressive properties. AIAA Journal 39(1):126–133. doi:10.2514/2.1280

28. Daniel IM, Werner BT, Fenner JS (2011) Strain-Rate-Dependent Failure Criteria for Composites. Composites Science and Technology In Press, Accepted Manuscript

29. Moulart R, Pierron F, Hallett S, Wisnom M (2011) Full-Field Strain Measurement and Identification of Composites Moduli at High Strain Rate with the Virtual Fields Method. Experimental Mechanics 1–28. doi:10.1007/s11340-010-9433-4

30. Hosur MV, Waliul Islam SM, Vaidya UK, Kumar A, Dutta PK, Jeelani S (2005) Dynamic punch shear characterization of plain weave graphite/epoxy composites at room and elevated temperatures. Composite Structures 70(3):295–307

31. Hosur MV, Islam SMW, Vaidya UK, Dutta PK, Jeelani S (2004) Experimental studies on the punch shear characterization of satin weave graphite/epoxy composites at room and elevated temperatures. Materials Science and Engineering A 368(1–2):269–279

32. Nemat-Nasser S, Isaacs JB, Starrett JE (1991) Hopkinson techniques for dynamic recovery experiments. Proc R Soc (London) A 435:371–391

33. Frew DJ, Forrestal MJ, Chen W (2002) Pulse shaping techniques for testing brittle materials with a split Hopkinson pressure bar. Experimental Mechanics 42(1):93–106

34. Subhash G, Nemat-Nasser S (1993) Dynamic stress-induced transformation and texture formation in uniaxial compression of zirconia ceramics. Journal of the American Ceramic Society 76(1):153–165

35. Klecka MA, Subhash G (2010) Rate-dependent indentation response of structural ceramics. Journal of the American Ceramic Society 93(8): 2377–2383

36. Ghosh D, Subhash G, Sudarshan TS, Radhakrishnan R, Gao X-L (2007) Dynamic indentation response of fine grained boron carbide. Journal of the American Ceramic Society 90(6):1850–1857

37. Meyers MA (1994) Dynamic behavior of materials, (Wiley)

38. Xiao JR, Gama BA, Gillespie JW Jr (2007) Progressive damage and delamination in plain weave S-2 glass/SC-15 composites under quasi-static punch-shear loading. Composite Structures 78 (2):182–196. doi:10.1016/j.compstruct.2005.09.001